JOURNAL OF COMPUTATIONAL PHYSICS 13, 130–157 (1973)

Two-Dimensional Implicit Radiation Hydrodynamics*

M. T. SANDFORD II AND R. C. ANDERSON

University of California, Los Alamos Scientific Laboratory, Los Alamos, New Mexico 87544

Received January 5, 1973

The equations describing a radiating gaseous medium are formulated in cylindrical geometry. These equations are the equations of hydrodynamics, the equation of radiative transfer, and the thermal equilibrium equation. A method for solving these that combines the work of Harlow and Amsden [1] and that of Fleck and Cummings [2] is presented. The radiation hydrodynamics of a hot bubble imbedded in cold air is used as a test problem. The bubble first cools by a radiative wave until its central temperature is about 1800 °K at 200 msec and then cools by means of hydrodynamic distortion. The bubble rises from its initial position in the atmosphere and forms into a torus that eventually thermalizes with the ambient air.

I. INTRODUCTION

Consider the equations describing an expanding, radiating, gaseous medium written in two-dimensional cylindrical geometry. We regard the gas as composed of one fluid (air for the present purposes). The gas properties are given by the thermodynamic variables T, the temperature; ρ the density; p_g, the gas pressure; p_e, the electron pressure; and I the specific internal energy. Regarding I and ρ as independent variables, one defines the equations of state which yield $p_g(I, \rho)$, and $T(I, \rho)$. These equations together with those giving other properties of the material (such as c_v, the specific heat, and κ_ν', the mass absorption coefficient corrected for stimulated emission) are collectively termed the "constitutive relations."

The equations of hydrodynamics express conservation in space and time of mass, energy, and momentum. The radial and axial fluid velocity components are denoted by u and v, respectively. The equations of hydrodynamics (1), (2), (3), (4) written in cylindrical Eulerian coordinates [1] express the conservation of mass (ρ), material

momentum (ρu, ρv), and total material energy density, (ρE); in a medium under uniform gravitational acceleration, g, in the negative z direction. The constants appearing in the equation set are:

$\bar{B}$ = heat conduction coefficient,
$\bar{\lambda}, \bar{\mu}$ = viscosity coefficients,

and

τ = mass diffusion coefficient.

Equations of Hydrodynamics in Cylindrical Eulerian Coordinates

Continuity Equation

$$\frac{\partial \rho}{\partial t} + \frac{1}{r}\frac{\partial \rho\, ur}{\partial r} + \frac{\partial \rho\, v}{\partial z} = \tau\left[\frac{1}{r}\frac{\partial}{\partial r} r\left(\frac{\partial \rho}{\partial r}\right) + \frac{\partial^2 \rho}{\partial z^2}\right]. \tag{1}$$

Momentum Equations

$$\frac{\partial \rho\, u}{\partial t} + \frac{1}{r}\frac{\partial \rho\, u^2 r}{\partial r} + \frac{\partial \rho\, uv}{\partial z} = -\frac{\partial}{\partial r}(p+q) + \bar{\mu}\frac{\partial}{\partial z}\left[\frac{\partial u}{\partial z} - \frac{\partial v}{\partial r}\right], \tag{2}$$

$$\frac{\partial \rho\, v}{\partial t} + \frac{1}{r}\frac{\partial \rho\, uvr}{\partial r} + \frac{\partial \rho\, v^2}{\partial z} = \rho g - \frac{\partial}{\partial z}(p+q) - \frac{\bar{\mu}}{r}\frac{\partial}{\partial r}\left[r\left(\frac{\partial u}{\partial z} - \frac{\partial v}{\partial r}\right)\right]. \tag{3}$$

Energy Equation

$$\begin{aligned}\frac{\partial \rho\, E}{\partial t} &+ \frac{1}{r}\frac{\partial \rho\, uEr}{\partial r} + \frac{\partial \rho\, vE}{\partial z} \\ &= \rho v g + \frac{1}{r}\frac{\partial}{\partial r}\left\{r\left[\bar{B}\bar{\mu}\frac{\partial I}{\partial r} - pu - \left(\frac{\bar{\lambda}}{\bar{\lambda}+2\bar{\mu}}\right)qu + \frac{\bar{\mu}}{2}\frac{\partial}{\partial r}(2u^2+v^2) + \bar{\mu}v\frac{\partial u}{\partial z}\right]\right\} \\ &+ \frac{\partial}{\partial z}\left\{\bar{B}\bar{\mu}\frac{\partial I}{\partial z} - pv - \left(\frac{\bar{\lambda}}{\bar{\lambda}+2\bar{\mu}}\right)qv + \frac{\bar{\mu}}{2}\frac{\partial}{\partial z}(u^2+2v^2) + \bar{\mu}u\frac{\partial v}{\partial r}\right]\right\},\end{aligned} \tag{4}$$

with

$$q = -(\bar{\lambda}+2\bar{\mu})\left(\frac{1}{r}\frac{\partial u\, r}{\partial r} + \frac{\partial v}{\partial z}\right).$$

The numerical values of $\bar{\lambda}$ and $\bar{\mu}$ define the compressional and shear components of the artificial viscous pressure. The ICE difference equations generally stabilize with less viscous pressure than required by explicit methods. The numerical value chosen for τ controls the amount of artificially introduced mass diffusion, and

we find a positive value is required to stabilize the equations with the small viscous pressure that is usually desired. The actual values of these parameters have no physical significance, and need only be large enough to give a stable calculation that does not smear the signals of interest. The ICE timestep and parameters are chosen according to the stability conditions given by Gentry [3]:

$$| \nabla \cdot \mathbf{v} | \Delta t_h \leqslant 0.1,$$

and

$$\tau = \bar{\mu} = \bar{\lambda} = (7/24) \max\{\delta r\, u_{\max}\,,\ \delta z\, v_{\max}\},$$

where $\mathbf{v}$ is the velocity vector; δr and δz, the radial and axial mesh spacing; and $u_{\max}$ and $v_{\max}$, the maximum radial and axial velocities.

The heat conduction coefficient $\bar{B}$ is regarded as constant since conduction is not an effective energy transport mechanism for the low densities we encounter. The ICE formulation does not time advance the energy equation, and the parameter $\bar{B}$ has been found useful as a means to introduce some diffusion required for stability. Equating $\bar{B}$ to the other parameters usually provides a stable solution.

To facilitate use of the computer code (SIERRA) written by Amsden to solve the hydrodynamics equations with the ICE method, we adopted the Local Thermodynamic Equilibrium [4] approximation. This implies that the radiation field is thermalized with the material and both have temperature T.

The temperature is found from the total energy that is calculated by solving Eq. (4):

$$E = I(T, \rho) + (1/2)(u^2 + v^2) + (u_r(T)/\rho), \tag{5}$$

where $u_r(T)$ is the radiation energy density. Hydrodynamic effects on the radiation field occur through temperature changes caused by changes in total energy E. The radiation field introduces a term in the momentum equations that we include by defining the total pressure

$$p = p_g + p_e + p_r \tag{6}$$

as the sum of gas, p_g, electron, p_e, and radiation, p_r, pressures. The absorption of radiation causes material heating that will increase the total pressure and affect the material motion through the momentum equations (2) and (3).

The radiation field is described by the monochromatic, specific intensity, $I_\nu(t; r, z; \theta, \omega)$. The angles θ and ω specify the direction vector $\mathbf{\Omega}$ shown in Fig. 1. The radiation energy density is defined by

$$u_r = \frac{1}{c} \int_0^\infty d\nu \int_0^{4\pi} I_\nu \, d\mathbf{\Omega}; \tag{7}$$

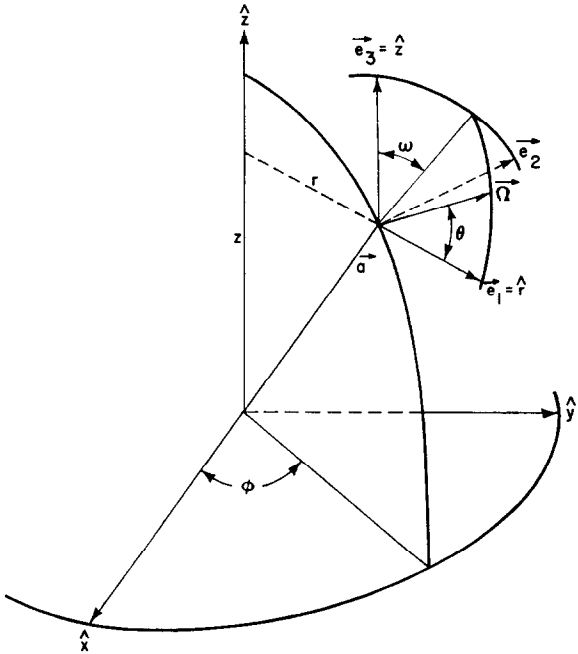

FIG. 1. The radiation field in cylindrical coordinates. The specific monochromatic intensity at **a** in the direction Ω is given as a function of ν, the frequency; r and z, spatial coordinates; θ and ω, photon flight direction coordinates; and t the time. The angle ω is measured in the plane containing $(\hat{e}_2, \hat{e}_3)$ from $\hat{e}_3$ to the projection of Ω in the plane.

and the radiation pressure by

$$p_r = \frac{1}{c}\int_0^\infty d\nu \int_0^{4\pi} I_\nu \cos^2\theta \, d\Omega. \tag{8}$$

We avoid calculating these moments of the specific intensity by approximating

$$I_\nu(t; r, z; \theta, \omega) \cong B_\nu[T(t, r, z)].$$

We obtain for Eqs. (7) and (8):

$$u_r \cong (4\pi/c)((\sigma/\pi)\, T^4) = aT^4, \tag{9}$$

and

$$p_r \cong (1/3)\, aT^4, \tag{10}$$

where a is the radiation density constant equal to 137.214 erg/cm^3 eV^4. These approximations are probably not serious since the intensity field must approach the

Planck function in optically thick regions where u_r and p_r can make significant contributions to E and p. The equation of radiative transfer (11) is written in cylindrical geometry (Fig. 1), and with the *LTE* assumption, Eq. (12) expresses the instantaneous conservation of the radiation field energy.

We divide a single timestep of the fluid into two parts:

I. Hydrodynamic motion with Δt_h.

II. Radiation transport with Δt_r.

Radiation Equations

Equation of Radiative Transfer

$$\frac{1}{c}\frac{\partial I_\nu}{\partial t} + L(I_\nu) = -\rho\kappa_\nu' I_\nu + \rho\kappa_\nu' B_\nu\,; \qquad I_\nu = I_\nu(t;\, \mathbf{a},\, \Omega), \tag{11}$$

Instantaneous Radiative Equilibrium

$$\frac{\partial(aT^4)}{\partial t} = \beta\left[\int_0^\infty d\nu \oint_0^{4\pi} d\Omega\ \sigma_\nu I_\nu - \int_0^\infty d\nu \oint_0^{4\pi} d\Omega\ \sigma_\nu B_\nu\right], \tag{12}$$

$$\sigma_\nu(T,\, \rho) = \rho\kappa_\nu'(T,\, \rho); \qquad \beta = \partial(aT^4)/\partial(\rho I).$$

In Cylindrical Coordinates:

$$L = \mu\frac{\partial}{\partial r} + (\sin\omega)(1-\mu^2)^{1/2}\frac{\partial}{\partial z} + \frac{(\cos^2\omega)(1-\mu^2)}{r}\frac{\partial}{\partial\mu} + \frac{\mu\sin\omega\cos\omega}{r}\frac{\partial}{\partial\omega}, \tag{13}$$

$\mu = \cos\theta.$

The total timestep considered is

$$\Delta t = \max(\Delta t_h\,, \Delta t_r),$$

and the temperature obtained from E after performing the hydrodynamic calculations is

$$\tilde{T}(t + \Delta t;\, r,\, z) = T(t;\, r,\, z) + \delta T_{\text{hydro}}\,,$$

which we regard as partially time advanced. This serves as the source temperature for the radiative transfer equation which is then solved to give the absorption:

$$\int_0^\infty d\nu \oint_0^{4\pi} d\Omega\ \sigma_\nu I_\nu\,.$$

Finally, the absorption is used in Eq. (12) to calculate the new, time advanced, temperature. The hydrodynamic timestep is defined by the stability criterion given previously, and the radiation timestep is defined by the prescription given in Section II. We generally find the hydrodynamic stability conditions result in $\Delta t_h < \Delta t_r$, and several ICE calculations are required to obtain $\tilde{T}$ values advanced by Δt.

II. Implicit Radiative Transfer

A time-implicit, one-dimensional, numerical solution for the equations of radiative transfer and instantaneous energy conservation has been presented by Fleck and Cummings [2]. This method combines an implicit difference approximation for Eq. (12) and a Monte Carlo solution of the radiative transfer equation (11). We have extended the Fleck method to two space dimensions, and the implicit equations resulting are:

$$\frac{1}{c}\frac{\partial I_\nu}{\partial t} + L(I_\nu) + \sigma_\nu I_\nu$$

$$= \frac{1}{4\pi}\left[\frac{\alpha\beta\,\Delta t_r\,\sigma_\nu b_\nu\,4\pi}{1+\alpha\beta c\,\Delta t_r\,\sigma_p}\right]\int_0^\infty d\nu' \oint_0^{4\pi} d\Omega\,\sigma_{\nu'} I_{\nu'} + \left[\frac{\sigma_\nu b_\nu}{1+\alpha\beta c\,\Delta t_r\,\sigma_p}\right] u_r^n, \quad (14)$$

and

$$T^{n+1} = \tilde{T} + \frac{\beta f}{4a(\tilde{T}^\gamma)^3}\left[\int_{t^n}^{t^{n+1}} dt \int_0^\infty d\nu \oint_0^{4\pi} d\Omega\,\sigma_\nu I_\nu - c\sigma_p\,\Delta t_r\,u_r^n\right]. \quad (15)$$

Our units are those conventionally employed for the specific radiation field [5] and this results in a Planck mean weighting function that differs from that of Fleck. We define the Planck mean absorption coefficient as:

$$\sigma_p = \frac{4\pi}{c}\int_0^\infty \sigma_\nu b_\nu d\nu\,, \quad (16)$$

with the "normalized Planck distribution":

$$b_\nu = \frac{B_\nu}{aT^4}\,; \qquad \int_0^\infty b_\nu\,d\nu = \frac{c}{4\pi}\,.$$

The "radiation derivative," β, is written as:

$$\beta = \partial u_r/\partial \rho I,$$

and is obtained in tabular form from numerical differentiation of the equation of state. The superscript γ in these equations indicates parametric[1] time-centering:

$$\hat{T}^{\gamma} = \alpha T^{n+1} + (1 - \alpha)\, \hat{T}. \tag{17}$$

The quantities appearing without superscripts or at t^n are taken as functions of $(\hat{T}, \rho)$ and are therefore hydrodynamically time advanced.

We may rewrite Eq. (14) in a more familiar form:

$$\frac{1}{c}\frac{\partial I_\nu}{\partial t} + L(I_\nu) = -\sigma_\nu I_\nu + \frac{1}{4\pi}\int_0^\infty d\nu' \oint_0^{4\pi} \Sigma_s(\nu', \nu)\, I_{\nu'}\, d\Omega' + \sigma_{\nu a} b_\nu u_r^n, \tag{18}$$

where we have defined the coefficient for scattering from frequency ν' to frequency ν as

$$\Sigma_s(\nu', \nu) = 4\pi[\alpha\beta\, \Delta t_r/(1 + \alpha\beta c\, \Delta t_r\, \sigma_p)]\, \sigma_{\nu'}\sigma_\nu b_\nu\,, \tag{19a}$$

and the absorption coefficient as

$$\sigma_{\nu a} = \sigma_\nu[1/(1 + \alpha\beta c\, \Delta t_r \sigma_p)]. \tag{19b}$$

The usual differential scattering coefficient is found by integrating Eq. (19a) over ν:

$$\sigma_{\nu' s} = \int_0^\infty \Sigma_s(\nu', \nu)\, d\nu,$$

or

$$\sigma_{\nu' s} = \sigma_{\nu'}[\alpha\beta c\, \Delta t_r \sigma_p/(1 + \alpha\beta c\, \Delta t_r \sigma_p)]. \tag{20}$$

One obtains the simple relations

$$\sigma_{\nu s} = \sigma_\nu(1 - f);\ \sigma_{\nu a} = \sigma_\nu f, \tag{21a,b}$$

and the scattering albedo is therefore $(1 - f)$, and depends upon the time advance used to solve the problem.

The consequence of using the implicit heat equation is therefore an equation of radiative transfer (18) with a scattering term in the source function. This term vanishes when the explicit limit ($\alpha = 0$) is used. One correlates the scattering term with the physical processes of instantaneous absorption and emission because this term represents the material emissivity at frequency ν due to absorption at ν'.

A fully implicit ($\alpha = 1$) radiative timestep Δt_r that gives stability to the solution can be obtained by requiring that the photon mean-free-path $1/\sigma_p$, approximately equal the photon thermalization distance $\beta c\, \Delta t_r$. For explicit ($\alpha = 0$) calculations, the photon flight distance $c\, \Delta t_r$, should approximately equal the mean-free-path.

[1] Note that $\hat{T}^{\gamma} = T^{n+1}$ when $\alpha = 1$, and the equation is fully implicit.

We have successfully employed the condition

$$1/\sigma_p \cong (1 - \alpha)\, c\, \Delta t_r + \alpha\beta c\, \Delta t_r\,, \tag{22}$$

or

$$\Delta t_r \cong 1/c\sigma_p[1 + \alpha(\beta - 1)]. \tag{23}$$

Using values typical for air at $T = 2000°\text{K}$ and $\rho = 1.3 \times 10^{-5}$ g/cm^3, we obtain

$$\Delta t_r(\alpha = 0) \cong 1.85 \times 10^{-4} \text{ sec}$$

$$\Delta t_r(\alpha = 1) \cong 123.5 \text{ sec}$$

which illustrates one advantage of the implicit formulation.

Equation (18) may solved by any convenient numerical method; viz a difference method such as S_n, the variable Eddington factor method, or the Monte Carlo method. Since the equation includes scattering, and because one does not require the monochromatic specific intensity, but rather its double integral [Eq. (15)], the last method is particularly appealing. The Monte Carlo solution of Eq. (18) proceeds in the usual sense, and we estimate

$$E_D(t; r, z) = \Delta t_r \int_0^\infty d\nu \oint_0^{4\pi} d\Omega\, f\sigma_\nu I_{\nu'} \text{ [erg/cm}^3\text{]}, \tag{24}$$

which is the absorption required in Eq. (15).

III. Radiative Transfer Solution

The Monte Carlo solution described here utilizes techniques motivated by the unique design features of the CDC 7600 computer; and, to a lesser extent, to features of the Chili Ridge Operating System (CROS) developed at Los Alamos.

Equation (18) is the integrodifferential equation to be solved by computing sample estimates of E_D from a suitable population of statistical particles. The random variables carried by each particle are E_p, the particle energy; ν, the particle frequency; t, the time; $\mathbf{a}(r, z, \phi)$, the particle position vector; and $\mathbf{\Omega}(\theta, \omega)$, the particle propagation direction unit vector. Figure 1 illustrates the relationship of $\mathbf{a}$ and $\mathbf{\Omega}$ to the cylindrical coordinate system.

The statistical source particles have initial coordinates distributed according to to the emission density appearing in the equation of radiative transfer (18):

$$\epsilon_\nu(t; r, z; \theta, \omega) = \sigma_{\nu a} b_\nu u_r^n,$$

which becomes, with the definitions of b_ν and (19b) of $\sigma_{\nu a}$:

$$\epsilon_\nu = f\sigma_\nu B_\nu(\tilde{T}), \qquad \text{erg/cm}^3 \text{ sec } sr\ d\nu. \tag{25}$$

The random walk of these particles follows the spacetime operator appearing on the left-hand side of Eq. (18):

$$G = (1/c)(\partial/\partial t) + L,$$

and the particle interactions with the material are the absorption and scattering mechanisms:

$$-\sigma_\nu I_\nu + \frac{1}{4\pi}\int_0^\infty d\nu' \int_0^{4\pi} \Sigma_s(\nu', \nu)\, I_{\nu'}\, d\Omega'.$$

IV. Source Particles

The total emitted energy in the computing mesh is

$$E_{\text{tot}}^n = \frac{c\,\Delta t_r}{4\pi}\int_0^R r\,dr \int_{-Z}^{+Z} dz\, f\sigma_p u_r^n. \tag{26}$$

Since the integrand is constant over a cell, we write

$$E_{\text{tot}}^n \cong \sum_{ij} E_{ij}^n\, \Delta V_{ij}\,, \tag{27}$$

where the volume of the cell is ΔV_{ij} , and

$$E_{ij}^n = (c\,\Delta t_r/4\pi)(f\sigma_p u_r^n)_{ij}\,.$$

The probability density function for energy emitted in cell (ij) is therefore approximated by

$$e(r_i\,, Z_j)\,\Delta V_{ij} \cong E_{ij}^n\,\Delta V_{ij}\Big/\sum_{ij} E_{ij}^n\,\Delta V_{ij} = E_{ij}^n\,\Delta V_{ij}/E_{\text{tot}}^n\,. \tag{28}$$

We may assign a fixed energy to each particle

$$E_p{}^n = E_{\text{tot}}^n/N_s{}^n, \tag{29}$$

where $N_s{}^n$ is the number of source particles begun during the timestep, and play

for the initial coordinates by rejection sampling the density function. Or, we may assign statistical particles to each cell (ij) in the number

$$N_{ij}^{n} = N_s^{n} e(r_i, z_j)\, \Delta V_{ij}, \tag{30}$$

and with energy

$$(E_p^{n})_{ij} = E_{ij}^{n}\, \Delta V_{ij}/N_{ij}^{n}. \tag{31}$$

We have successfully employed both approaches, but find that biasing the density function is generally required to increase the efficiency of rejection sampling. In some cases, σ_p shows a strong maximum in temperature gradients and biasing by $1/\sigma_p$ can be advantageous.

The initial propagation direction unit vector is selected from the isotropic density function:

$$p(\theta, \omega)\, d\theta\, d\omega = \sin\theta\, d\theta\, d\omega. \tag{32}$$

Equation (25) shows that source particles are to be emitted at the time t^n with frequencies distributed according to the probability density function

$$p(\nu)\, d\nu = f\sigma_\nu B_\nu(\tilde{T})\, d\nu \Big/ f\int_0^\infty \sigma_\nu B_\nu(\tilde{T})\, d\nu,$$

or, using (16),

$$p(\nu)\, d\nu = (4\pi\sigma_\nu/cu_r^{n}\sigma_p)\, B_\nu(\tilde{T})\, d\nu. \tag{33}$$

The distribution function for the emission probability of frequency ν is therefore:

$$F(\nu) = \frac{4\pi}{c\sigma_p u_r^{n}} \int_0^\nu \sigma_{\nu'} B_{\nu'}(\tilde{T})\, d\nu'. \tag{34}$$

This density function can be sampled by using a rejection technique on tables of the density function computed for each mesh cell.

An alternative rejection sampling scheme for (33) is based upon a prescription given by Cashwell and Everett [6]. Write:

$$p(\nu)\, d\nu = \tilde{\sigma}_\nu(\sigma_m B_\nu(\tilde{T})/(c/4\pi)\, \sigma_p u_r^{n})\, d\nu, \tag{35}$$

where

$$\tilde{\sigma}_\nu = \sigma_\nu/\sigma_m,$$

and

$$\sigma_m = \max_{0 \leqslant \nu \leqslant \infty} (\sigma_\nu).$$

Then one has $0 \leqslant \tilde{\sigma} \leqslant 1$, and the prescription samples the frequency from the distribution function

$$F_B(\nu) = \frac{4\pi\sigma_m}{c\sigma_p u_r^n} \int_0^\nu B_{\nu'}(T^n)\, d\nu', \tag{36}$$

and accepts the sample with probability $\gamma \leqslant \tilde{\sigma}_\nu$. A convenient scheme for sampling the density function

$$h(\nu')\, d\nu' = (4\pi/cu_r^n)\, B_{\nu'}(T)\, d\nu', \tag{37}$$

has been given by Barnett and Canfield as reported in Fleck and Cummings (cf. Cashwell's R. C23). Given here without proof, set

$$K = \min \left\{ k \ni \sum_{j=1}^{k} j^{-4} \geqslant \gamma\zeta(4) \right\}, \tag{38a}$$

where ζ is the zeta function and γ is uniformly random on (0, 1). Then one obtains

$$\nu = -\frac{1}{K} \ln \prod_{i=1}^{4} \gamma_i . \tag{38b}$$

V. The Scattering Interaction

Equation (18) contains the scattering source term

$$J_\nu(t; r, z; \Omega) = \frac{1}{4\pi} \int_0^\infty d\nu' \oint_0^{4\pi} d\Omega'\, \Sigma_s(\nu', \nu)\, I_{\nu'} . \tag{39}$$

which governs the Monte Carlo modeling of the collision interaction. Integrating (39) over ν yields

$$\int_0^\infty d\nu\, J_\nu(t, r, z; \Omega) = \frac{(1-f)}{4\pi} \int_0^\infty d\nu' \oint_0^{4\pi} d\Omega'\, \sigma_{\nu'} I_{\nu'} , \tag{40}$$

which shows the effective scattering to be isotropic, and nonconservative. We account for the effective absorption in the medium by exponentially attenuating the statistical particles' energy between collisions. Thus, the energy fraction that scatters follows the probability distribution function isotropic in direction and varying in frequency as:

$$P(\nu) = \int_0^\nu d\nu'\, J_{\nu'} \Big/ \int_0^\infty d\nu'\, J_{\nu'} . \tag{41}$$

By using the condition of static radiative equilibrium we obtain:

$$\frac{1}{4\pi}\int_0^\infty d\nu \oint_0^{4\pi} d\Omega'\ \sigma_\nu I_\nu = \frac{1}{4\pi}\int_0^\infty d\nu \oint_0^{4\pi} d\Omega'\ \sigma_\nu B_\nu ,$$

From which we infer a modeling for the integrated mean intensity:

$$\int_0^\infty d\nu\ J_\nu \cong (1-f)\int_0^\infty d\nu\ \sigma_\nu B_\nu . \tag{42}$$

One therefore approximates the equation for $P(\nu)$ as:

$$P(\nu) = \int_0^\nu \sigma_{\nu'} B_{\nu'}\, d\nu' \Big/ \int_0^\infty \sigma_{\nu'} B_{\nu'}\, d\nu',$$

or simply

$$P(\nu) = F(\nu),$$

which is the same Kirchhoff's law distribution function previously employed for sampling source particle frequencies. The scattering interaction then results in the following prescription:

(A) selection of Ω uniform over $4\pi sr$,
(B) selection of a new frequency from $P(\nu)\, d\nu$,
(C) selection of a new collision distance (Eq. (45)).

VI. The Random Walk

The walk geometry is governed by the operator L, which expresses the intensity divergence in cylindrical coordinates. As a particle travels along its random walk in space and time, it deposits energy between collisions in the amount

$$\Delta E(t; r, z) = E_p(t)[1 - \exp(-\sigma_{\nu a} \mid \mathbf{a}_j - \mathbf{a}_{j-1} \mid)], \tag{43}$$

where $\mathbf{a}_j$ is the vector to the jth interaction (collision), $\mathbf{a}_{j-1}$ is the vector to the previous one, and E_p is the instantaneous particle energy. The extinction originates with the $-\sigma_\nu I_\nu$ term in the equation of transfer (18), and the expression above represents the intensity attenuation due to the effective absorption, since

$$\sigma_\nu = \sigma_{\nu a} + \sigma_{\nu s} . \tag{44}$$

The distance between collisions is a random variable sampled from

$$d_{\text{col}} = \mid \ln(\gamma) \mid /(1-f)\ \sigma_\nu , \tag{45}$$

and the walk from $\mathbf{a}_{j-1}$ to $\mathbf{a}_j = \mathbf{a}_{j-1} + d_{\text{col}}\Omega_j$ may require traversing several mesh cells. The mesh variables and constitutive relations are stored in tabular form and double-linear[2] interpolation is used to obtain any mesh quantity: viz, f and σ_ν required by Eq. (45).

Let us assume that a particle is to be propagated from **a** to **b**, as shown in Fig. 2. The total energy deposited by the particle will be approximated by

$$\Delta E = \Delta E_1 + \Delta E_2 + \Delta E_3 ,$$

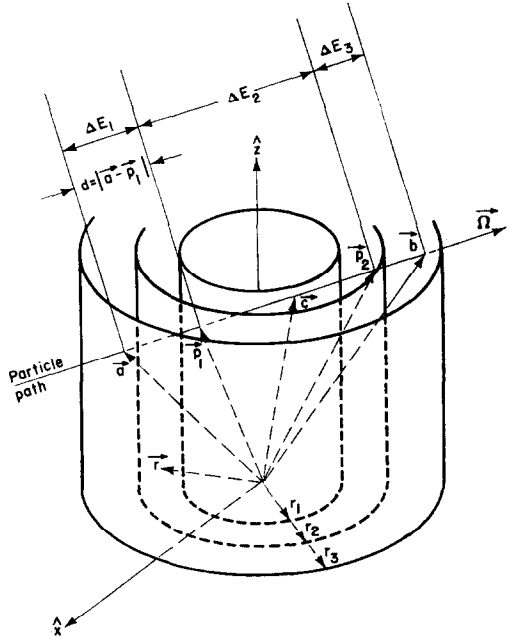

FIG. 2. Particle path geometry. A statistical particle moving from **a** to **b** intersects cylindrical mesh cell boundaries at $\mathbf{p}_1$ and $\mathbf{p}_2$, and the energy loss $\Delta E_{1,2,3}$ at **c**, the midpoint in the flight path.

where ΔE_1 is that lost along $\mathbf{a} - \mathbf{p}_1$, ΔE_2 is that lost along $\mathbf{p}_1 - \mathbf{p}_2$, and ΔE_3 is the energy lost along $\mathbf{p}_2 - \mathbf{b}$. The vectors $\mathbf{p}_{1,2}$ are shown as vectors to the intersection of the particle path with a radial mesh boundary. The energy score is required as a function of position, but not time, and we therefore ignore the time dependence of $(\Delta E_k, k = 1, 2, 3)$ and score the estimate[3] at position **c**:

$$\Delta E(\mathbf{c}) = \Delta E((\mathbf{a} + \mathbf{b})/2) \cong \Delta E_1 + \Delta E_2 + \Delta E_3 ,$$

[2] Logarithmic interpolation is used to obtain constitutive relations.

[3] In cases with little effective scattering, it may be advantageous to score the individual ΔE_i, $(i = 1, 2, 3, \ldots, N)$.

where, for this example, Eq. (43) yields

$$\Delta E_1 = E_p[1 - \exp(-\sigma_{va} \mid \mathbf{a} - \mathbf{p}_1 \mid)],$$
$$\Delta E_2 = (E_p - \Delta E_1)[1 - \exp(-\sigma_{va} \mid \mathbf{p}_1 - \mathbf{p}_2 \mid)],$$

and

$$\Delta E_3 = (E_p - \Delta E_1 - \Delta E_2)[1 - \exp(-\sigma_{va} \mid \mathbf{p}_2 - \mathbf{b} \mid)].$$

If at any time during its propagation the particle energy falls to 1 % or less of its birth energy E_p^n, it is considered to have "died," its remaining energy rate is scored, and the particle history terminates.

During its walk from **a** to **b**, the particle advances time by an amount

$$\delta t = d_{\text{col}}/c. \tag{46}$$

No particle is permitted to travel a total distance greater than that required to advance one time step:

$$d_{\text{cen}} = c\,\Delta t, \tag{47}$$

which is called the "census" distance. Every particle travels until it either dies and is terminated, or until it reaches census. In the latter case, the particle's random variables at census are saved and the particle history is continued at the next time step. The computer code performs random walks for the census particles left from previous time steps before creating and following new source particles.

Clearly one requires scalar distances of the form $\mid \mathbf{a} - \mathbf{p}_1 \mid$ to step particles through the mesh. The vector $\mathbf{p}_1$ may, of course, represent an intersection with either a cylindrical boundary or with a plane of constant z. The equations for both intersections are derived below [7].

A. *Cylindrical boundary*

The equation of a cylinder (Fig. 2) is

$$\mathbf{r} = r\cos\phi\hat{x} + r\sin\phi\,\hat{y} + z\hat{z}, \tag{48}$$

and that for the intersecting line is

$$\mathbf{r} = \mathbf{a} + \boldsymbol{\Omega} d,$$

or

$$\mathbf{r} = (a_1 + \Omega_1 d)\,\hat{x} + (a_2 + \Omega_2 d)\,\hat{y} + (a_3 + \Omega_3 d)\,\hat{z}. \tag{49}$$

Intersection at $\mathbf{p}_1$ requires

$$z = \mathbf{r} \cdot \hat{z} = a_3 + \Omega_3 d, \tag{50a}$$

and

$$\mathbf{r}^2 = r^2 + z^2. \tag{50b}$$

Substituting (49) into (50b) and using (50a) to solve d yields

$$d = \frac{-(a_1\Omega_1 + a_2\Omega_2) \pm [(a_1\Omega_1 + a_2\Omega_2)^2 - (\Omega_1^2 + \Omega_2^2)(a_1^2 + a_2^2 - r^2)]^{1/2}}{(\Omega_1^2 + \Omega_2^2)}. \tag{51}$$

The desired distance is the least, positive value given by (51).

B. *Intersection with a z plane (Fig. 3)*

The equation of the plane is

$$\mathbf{r} \cdot \hat{z} = z, \tag{52}$$

into which (49) is substituted to yield

$$a_3 + \Omega_3 d = z,$$

or

$$d = (z - a_3)/\Omega_3 . \tag{53}$$

An algorithm (TDIST) is used by the computer code to determine the distance to the nearest cell boundary, d; along the direction, $\mathbf{\Omega}$; from the point, $\mathbf{a}$.

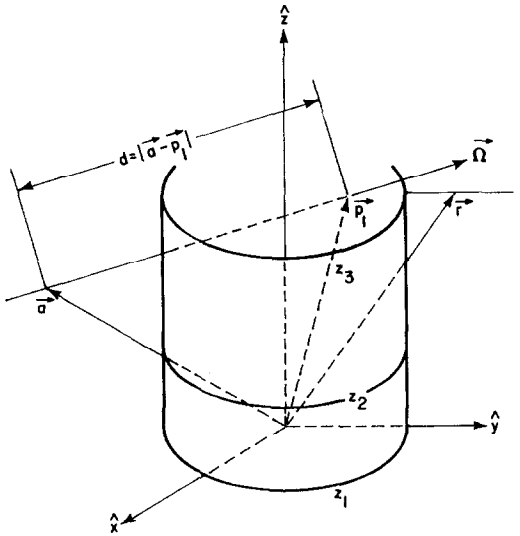

FIG. 3. Intersection of the flight path with direction $\mathbf{\Omega}$ and a plane boundary at $\mathbf{p}_1$. The distance from the starting point $\mathbf{a}$, to $\mathbf{p}_1$ is d; and $\mathbf{r}$ is a vector to the plane with coordinate z_3.

The random walks are performed in the REEFER computer code by a subroutine, WALK, which randomly walks a particle, having an initial energy E, and frequency ν_p ; from $\mathbf{a}(r, z, \phi)$ in the initial direction Ω, to either its "death" by energy loss or escape from the mesh, or to the census distance. The ultimate fate of the particle (death or census) is indicated by a variable IDIE which has values

$$\text{IDIE} = 0, \text{ indicating particle death,}$$

or

$$\text{IDIE} = 1, \text{ indicating arrival at census.}$$

A flow diagram of this subroutine is shown in Fig. 4.

During the course of a particle's random walk, the value of IDIE is set at -1 to indicate that its frequency ν_p , does not change during its walk between collisions (Fig. 2). The cylindrical coordinates of the particle (r_p , z_p) are found from its vector position $\mathbf{a}$, by subroutine PLACE. Single entry tables are searched to find the index k, such that

$$x_k \leqslant x < x_{k+1} ,$$

where x is the argument for interpolation into any table of values

$$y_j(x_j), \qquad (j = 1, 2, 3,..., N).$$

The index, k is found by subroutine SEARCH which performs a Boolean, binary search. Double entry tables are interpolated by the function DBLINT which performs double-linear interpolation [8].

The energy deposition (absorption) estimates from the random walks are stored in the array EDEP, which allows NBUF number sets $(r, z, \Delta E, \nu)$ to be stored in the computer memory. When the counter ID exceeds NBUF, the array is dumped to the disk storage by subroutine FLUSH, thereby freeing the memory storage space. The energy samples stored on the disk are retrieved after each time step and used to advance the mesh temperatures. The CROS76 operating system [9] allows information stored on the computer disk to be staged to magnetic tapes during computation, thereby freeing the disk storage space. At the completion of a time step, the energy depositions are staged to magnetic tape for archival storage and use in later calculations by other codes. The particles that escape the mesh are tallied separately to yield the time-dependent radiative power output.

VII. Temperature Advancement

After randomly walking the census and source particles for each mesh cell, one accumulates a spatial distribution of scores $\Delta E_k(r, z)$, and frequencies ν_k , $(k = 1, 2, 3,..., N)$. These are stored on the computer disk storage device since their number N, exceeds the computer memory capacity. The radiative shock fronts

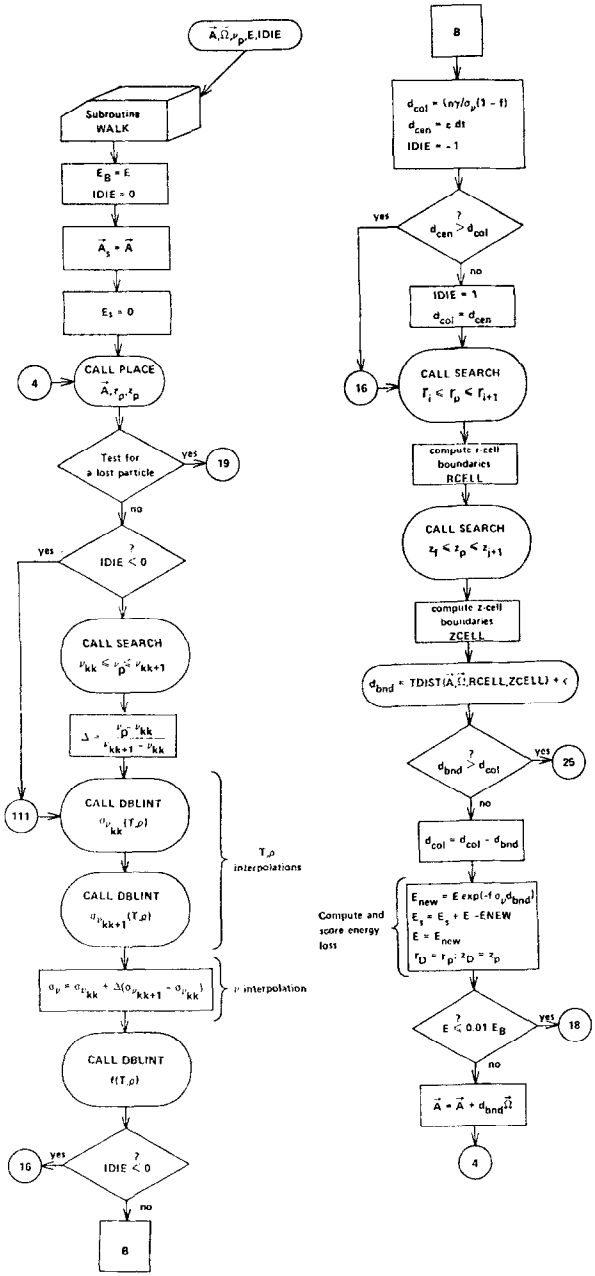
$\vec{A},\vec{\Omega},\nu_p,E,IDIE$
Subroutine WALK
$E_B = E$
IDIE = 0
$\vec{A}_s = \vec{A}$
$E_s = 0$
4
CALL PLACE
$\vec{A}, r_p, z_p$
Test for a lost particle
yes
19
no
IDIE < 0 ?
yes
CALL SEARCH
$\nu_{kk} \leq \nu_p \leq \nu_{kk+1}$
$\Delta = \frac{\nu_p - \nu_{kk}}{\nu_{kk+1} - \nu_{kk}}$
111
CALL DBLINT
$\sigma_{\nu_{kk}}(T,\rho)$
CALL DBLINT
$\sigma_{\nu_{kk+1}}(T,\rho)$
T,ρ interpolations
$\sigma_p = \sigma_{\nu_{kk}} + \Delta(\sigma_{\nu_{kk+1}} - \sigma_{\nu_{kk}})$
ν interpolation
CALL DBLINT
f(T,ρ)
16
yes
IDIE < 0 ?
no
8
8
$d_{col} = (n\gamma/\sigma_p(1-f)$
$d_{cen} = c\,dt$
IDIE = -1
yes
$d_{cen} > d_{col}$?
no
IDIE = 1
$d_{col} = d_{cen}$
16
CALL SEARCH
$r_i \leq r_p \leq r_{i+1}$
compute r-cell boundaries RCELL
CALL SEARCH
$z_j \leq z_p \leq z_{j+1}$
compute z-cell boundaries ZCELL
d_{bnd} = TDIST($\vec{A},\vec{\Omega}$,RCELL,ZCELL) + ε
$d_{bnd} > d_{col}$?
yes
25
no
$d_{col} = d_{col} - d_{bnd}$
Compute and score energy loss
$E_{new} = E\exp(-f\sigma_p d_{bnd})$
$E_t = E_s + E - ENEW$
$E = E_{new}$
$r_D = r_p$; $z_D = z_p$
$E \leq 0.01\,E_B$?
yes
18
no
$\vec{A} = \vec{A} + d_{bnd}\vec{\Omega}$
4

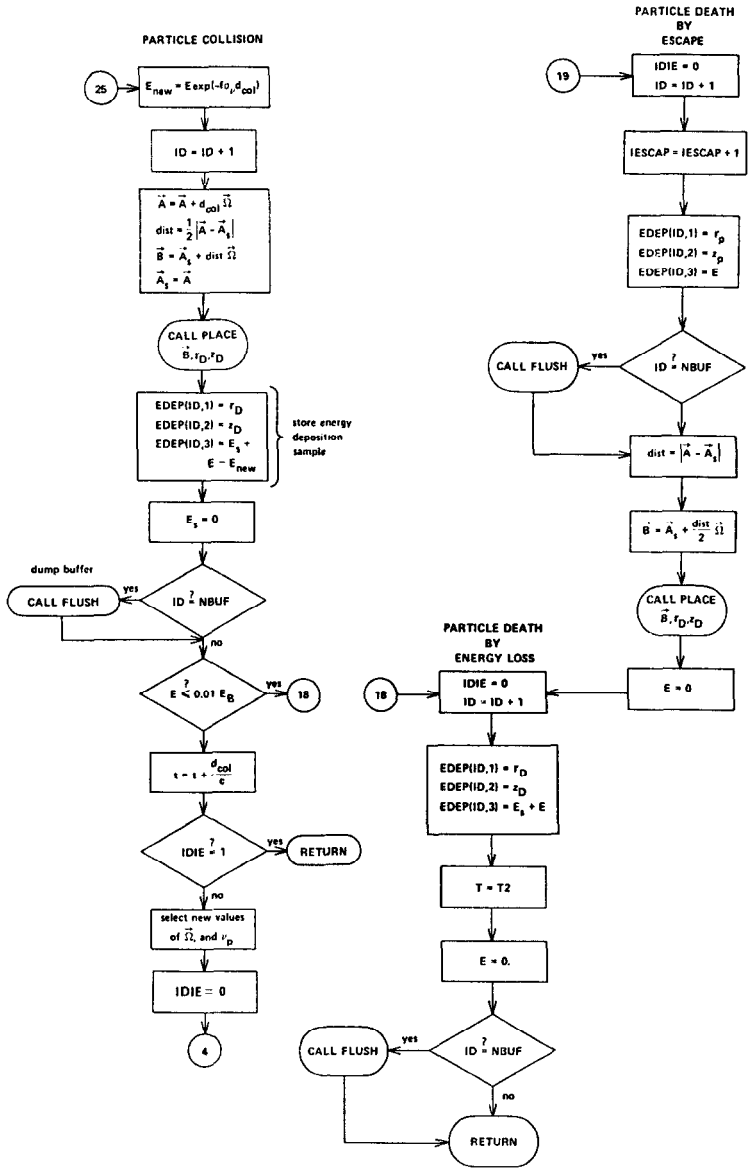

FIG. 4. Flow diagram for the computation of a statistical particle random walk. The particle begins the walk with coordinates **A**, flight direction Ω, frequency ν_p, and energy E. The particle fate is given by the computed variable IDIE.

are therefore resolved with the statistical precision of these estimates which are ultimately saved on magnetic tapes.

The temperature advancement via Eq. (15) proceeds with the mesh resolution, since the gas dynamics are not strongly affected by a loss of spatial resolution in the radiative shock temperature structure. Clearly, the computation of intensities from the source function, $B_\nu[T; r, z)]$, requires resolution of the temperature gradients; and the individual energy scores are thus preserved for this later calculation.

To obtain the total radiation power deposited (absorbed) in a cell, it is only necessary to recover (from the disk storage) blocks of energy samples and form the restricted sums of the $N(ij)$ samples in each cell:

$$\xi_{ij} = \sum_{k=1}^{N(ij)}{}' \Delta E_k(r, z); \qquad (i = 1, 2, 3,..., N_r\,; \quad j = 1, 2, 3,..., N_z), \tag{54}$$

where the prime denotes restriction of r and z to the cell (i, j):

$$(r_i - \Delta r^-) \leqslant r \leqslant (r_i + \Delta r^+), \tag{55a}$$

and

$$(z_j - \Delta z^-) \leqslant z \leqslant (z_j + \Delta z^+), \tag{55b}$$

where r_i and z_j are the coordinates of the cell center, and Δr and Δz are the half distances to the centers of adjacent cells. Thence, Eq. (15) becomes

$$T_{ij}^{n+1} = \tilde{T}_{ij} + \frac{\beta_{ij}\,\Delta t_r}{4a(\tilde{T}_{ij}^{\,v})^3}\left[\frac{\xi_{ij}}{\Delta V_{ij}} - acf_{ij}\sigma_{p,ij}(\tilde{T}_{ij})^4\right], \tag{56}$$

and serves to advance the temperatures in the mesh.

VIII. The Diffusion Limit

The condition of radiation diffusion is naturally achieved by the Implicit Monte Carlo Method. This limit obtains when the photon mean-free-path is much shorter than the thermalization distance:

$$1/\sigma_p \ll \alpha\beta c\,\Delta t_r\,, \qquad \text{and} \qquad f \ll 1. \tag{57}$$

In this limit, the effective scattering becomes nearly conservative, and since the loss between collisions is [Eq. (43)]:

$$\Delta E = E_p(1 - e^{-f\sigma_p \Delta X}),$$

the particles may not lose their energy very quickly. For only a few frequencies $\sigma_\nu \Delta X$ may be large compared to the absorption fraction; and situations occur with much particle scattering and little absorption, resulting in an excessive expenditure of computing time. Several solutions to this problem have been posed:

1. use of the diffusion approximation in optically thick regions;
2. use of a grey IMC calculation in thick regions;
3. use of importance biasing (splitting and Russian roulette) in thick regions.

The second of these solutions has been found most effective [10], although the third has not been fully explored. Since the large effective scattering in optically thick regions gives difficulties only for particle frequencies where $\sigma_\nu \Delta X$ is large compared to f, one can perform a grey calculation in these regions by using σ_p rather than σ_ν in the sampling Eq. (52). Then there results for the optical path between collisions:

$$\Delta\tau = f\sigma_p \Delta X = \sigma_p \Delta X/(1 + \alpha\beta c\sigma_p \Delta t_r), \tag{58}$$

or

$$f\sigma_p \Delta X = \Delta X/((1/\sigma_p) + \alpha\beta c \Delta t_r). \tag{59}$$

Since $\sigma_p \gg \alpha\beta c \Delta t$ we select ΔX so that

$$f\sigma_p \Delta X \cong \Delta X/\alpha\beta c \Delta t_r \cong 1,$$

and although the scattering is nearly conservative, the particles are rapidly attenuated between collisions. There are, of course, particles that reach census or leave the optically thick regions, and we therefore sample and retain the frequency. The mean absorption coefficient is simply employed in place of the monochromatic value if the scattering fraction f, is above some limit at the coordinates of interest.

Importance biasing provides another alternative since the radiative energy transport in the optically thick (diffusion) regions is not as large as in the thin regions because the temperature gradient is generally not steep. The optically thin regions are therefore more important because the absorption coefficient is a sensitive function of the temperature; these regions act as an optical "valve" [11] to release the radiation of the hotter material.

One may assign "importance" numbers to the mesh cells [12]. These numbers indicate the biasing applied to a particle entering the cell. Let B_k be the importance number interpolated to a particle's kth collision point (r, z). The biasing applied to the random walk is as follows:

$B_k \geqslant B_{k-1}$: "Splitting." The particle is split into N particles, each having energy $(1/N) E_p$. One of the N particles continues in the random walk, and the others become branches of a particle tree that must be processed subsequent to the parent history.

$B_k < B_{k-1}$: "Russian Roulette." The particle history is continued with a probability p with an energy of $(1/p)\,E_p$. One continues the history if

$$\gamma \geqslant (1 - p),$$

where γ is uniformly random on (0, 1).

The optical thickness of the material is gauged by the albedo for effective scattering

$$\tilde{\omega}_0 = 1 - f,$$

and one might employ the scattering fraction, f, as the importance number.

IX. Numerical Example

The problem chosen to test the numerical method and computer code described in the previous sections consists of a hot, expanding, spherical bubble imbedded in an exponential atmosphere. The initial ($t = 0$) velocity, temperature, and density follow laws linear in the radius from the bubble center:

$$\begin{aligned} V(R) &= (R/R_0) \times 10^5 \text{ cm/sec}, \qquad R \leqslant R_0\,, \\ &= ((R_1 - R)/(R_1 - R_0)) \times 10^5 \text{ cm/sec}, \qquad R_0 \leqslant R \leqslant R_1\,, \\ &= 0, \qquad R > R_1\,. \end{aligned}$$

$$\begin{aligned} T(R) &= (R/R_0)(T_1 - T_C) + T_C\,, \qquad R \leqslant R_0\,, \\ &= T_1\,, \qquad R > R_0\,. \end{aligned}$$

$$\begin{aligned} \rho(R) &= (R/R_0)(\rho_1 - \rho_C) + \rho_C\,, \qquad R \leqslant R_0\,, \\ &= \rho_1\,, \qquad R > R_0\,. \end{aligned}$$

In these formulas, the central temperature kT_C , and density ρ_C , are taken as 1.0 eV and 1.291×10^{-6} g/cm^3; and the ambient values are $kT_1 = 0.02586$ eV and $\rho_1 = 1.291 \times 10^{-3}$ g/cm^3. The velocity increases linearly from zero at the bubble center to 10^5 cm/sec at R_0 , the thermal "edge," and falls linearly to zero at R_1 . We have taken R_0 and R_1 as 1500 and 2000 cm, respectively. The initial values at cylindrical mesh cell centers with coordinates $(r_i\,, z_j)$ therefore correspond to those at the radius:

$$R_{ij} = r_i^2 + z_j^2.$$

The constitutive relations consist of equations of state provided by Merts and McGee [13] and air opacities taken from Harris [14]. The latter consist of tables logarithmic in temperature (25 points) and density (8 points), and linear in photon frequency (500 points).

This calculation was performed with 1300 computing cells arrayed to form a 26×50, $r - z$ mesh. Figure 5 shows the initial conditions for this problem. The marker particles are Lagrangian fluid particles that serve to indicate the motion of the fluid; they do not interact in the Eulerian fluid calculation. The velocity plot indicates the fluid direction and speed relative to the mesh maximum of each mesh cell center. The temperature and density are each shown as a surface above the $r - z$ plane, and the time evolution of the bubble is followed by examining a sequence of these plots.

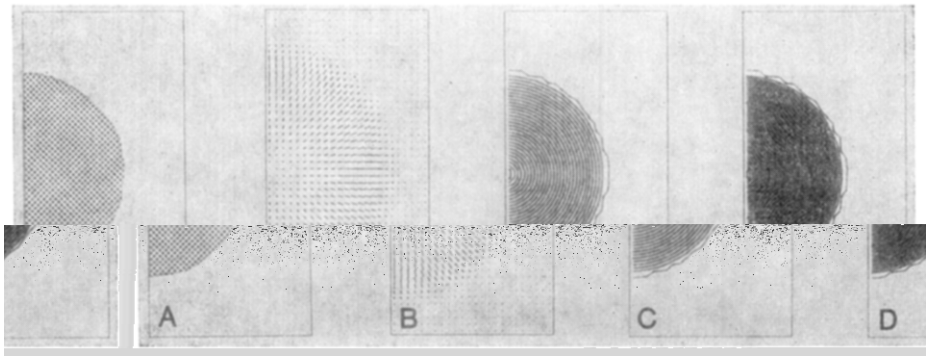

FIG. 5. Test problem initial conditions: (5a) fluid marker particles; (5b) fluid velocities; (5c) fluid temperatures (decreasing from center); (5d) fluid densities (increasing from center).

The bubble quickely expands to fill the Eulerian mesh, and the computer code therefore performs a "rezone" procedure that doubles the mesh size when signals propagate to the boundary. The rezone procedure was executed three times at 1.44, 25.0, and 108 msec, giving cell sizes that ranged from 100 cm, initially, to 800 cm at late times. The radiation calculations were performed with approximately 2000 new source particles in each time step. The time step Δt_R, chosen for the radiation calculations produced about five steps per decade of time, and no stability problems were encountered with the IMC method. The ICE method stability requires that its time step be taken to satisfy the conditions obtained by Gentry [3], and it is therefore necessary to perform several hydrodynamic time steps for each radiation calculation. This number varied from one (initially) to about 50 (at later times).

The temperature history for the fluid is demonstrated in Fig. 6 which shows the maximum mesh temperature at various times. The initial cooling is by radiation and occurs in the form of a wave that moves inward. During this phase of the evolution, a shock develops, and produces expansion that further reduces the central density. The radiation field initially increases the central temperature

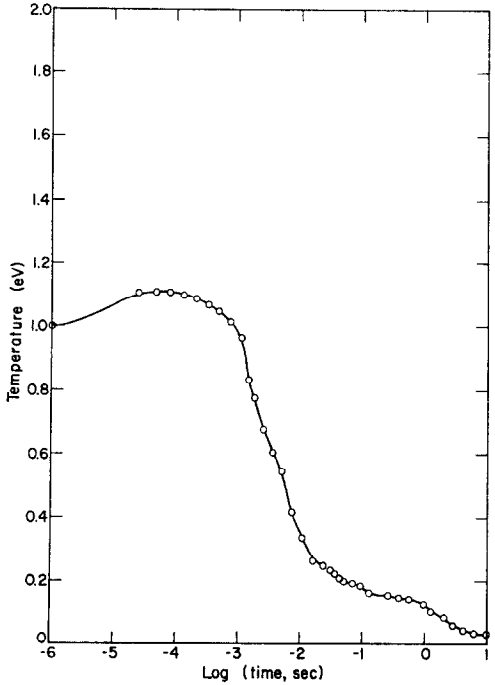

FIG. 6. Maximum mesh cell temperature in ev versus time in seconds.

(Fig. 6). The outer portions of the bubble then radiate away energy until a central core of about 0.5m radius and 0.7 eV temperature remains at 2 msec. The wave reaches the center at about 16 msec, at which time the central temperature is 0.25 eV and the bubble is optically thin. The temperature–time curve changes slope at this time and the cooling to a time of about 1 sec results from the combined effects of infrared radiation and hydrodynamic expansion. The cooling at late times ($t > 5$ sec) is purely hydrodynamic and arises from the energy lost by work done to form, expand, and raise the torus.

The motion of the radiative wave is clearly seen in Fig. 7 even though irregularities develop in the mesh from statistical variations introduced by the Monte Carlo calculations. The bubble remains nearly spherical during the radiative cooling phase, and the hydrodynamic shock advances to a radius of 4800 cm. The bubble distortion and torus formation at 1 sec and later is easily seen in the marker particle plots. The computing mesh is moved upward by the rezone procedure and the bubble rise is therefore not obvious in these plots.

Statistical particles that leave the mesh during each timestep are employed to estimate the frequency integrated (thermal) power radiated by the bubble. The

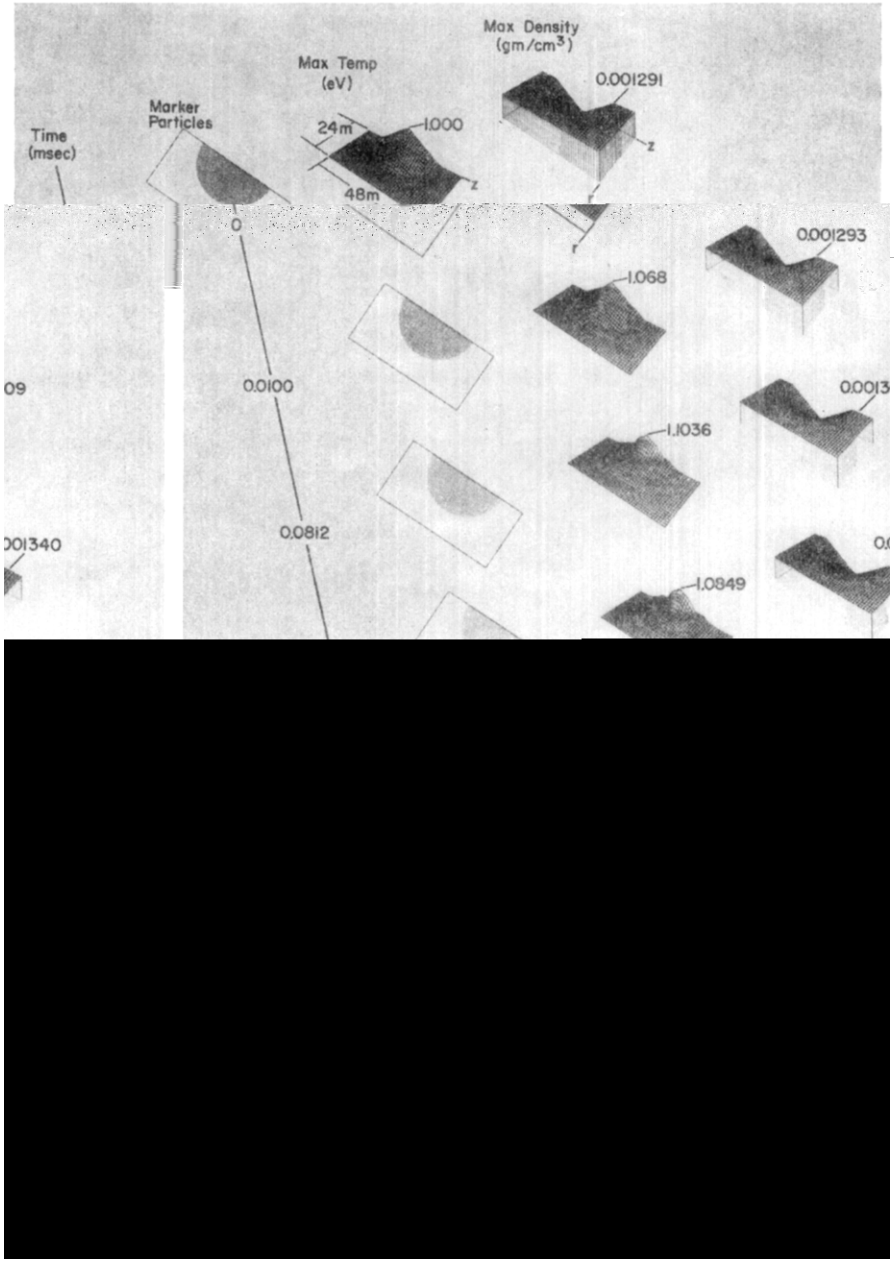

FIG. 7. Time evolution of the fluid shown by marker particles, temperatures, and densities Note that the plotting scales are not constant with time.

FIG. 7a. Fluid history from initial conditions to 1.13 msec.

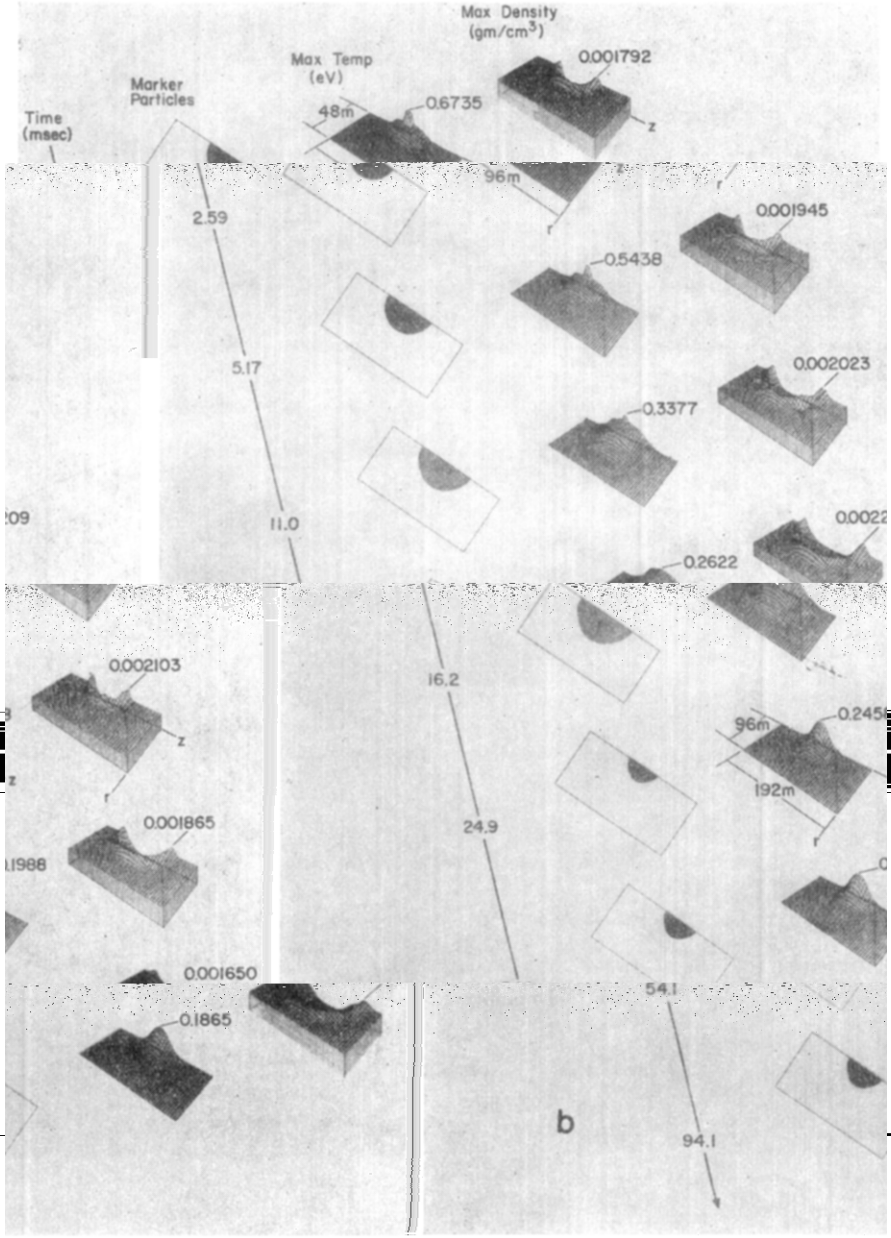

FIG. 7b. Fluid history from 2.59 to 94.1 msec.

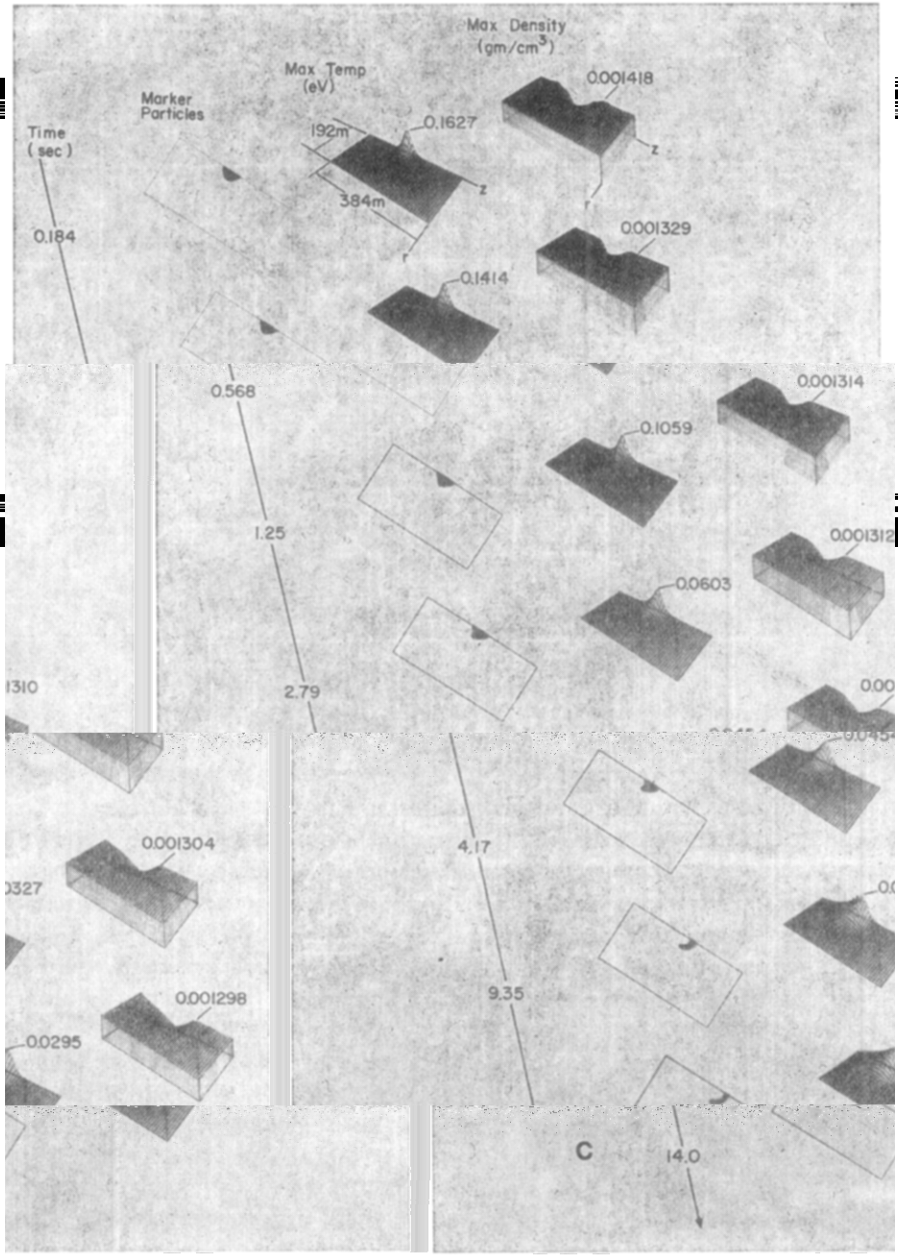

FIG. 7c. Fluid history from 0.184 to 14.0 sec.

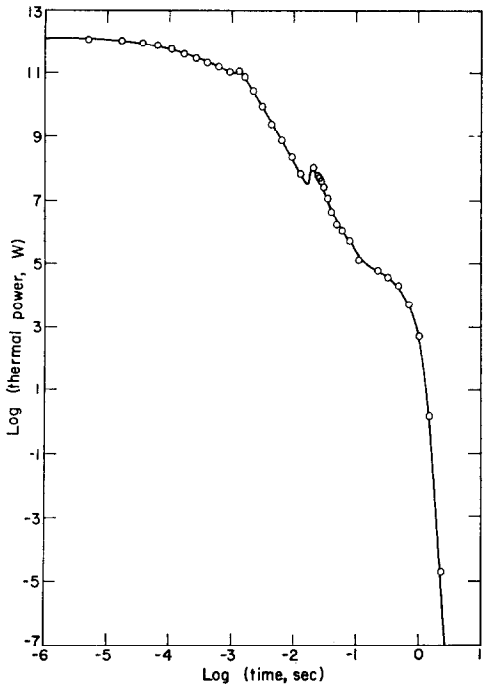

FIG. 8. Thermal power–time curve for the hot bubble radiation.

resulting power time curve (Fig. 8) shows the thermal power is approximately constant at about 10^5 megawatts while radiation heats the bubble center in the first msec of time. The small discontinuities in the curve are generated by the rezone procedure which adds ambient air energy to the mesh that is then radiated away in the next few timesteps. The slope change occurring at 0.1 sec is real and marks the change from radiative to hydrodynamic cooling. The thermal output from the bubble is negligible at later times and the final temperature decrease (Fig. 6) is purely due to adiabatic cooling. The radiation spectrum, although not presented here, is easily obtained by also tallying the frequencies of particles leaving the mesh in each timestep.

The cooling wave phenomenon has been previously noted and discussed by Zel'dovich and Raizer [15].

ACKNOWLEDGMENTS

Our work has been performed with the valuable assistance of Drs. J. A. Fleck, R. A. Gentry, and E. M. Jones. We thank Drs. H. G. Horak and J. Zinn for many valuable discussions, and Drs. D. M. Kerr and H. Hoerlin for continuous encouragement. This work has been supported by the Los Alamos Scientific Laboratory under contract to the U. S. Atomic Energy Commission.

REFERENCES

1. F. HARLOW AND A. A. AMSDEN, *J. Comp. Phys.* **8** (1971), 197.
2. J. A. FLECK AND J. D. CUMMINGS, *J. Comp. Phys.* **8** (1971), 313.
3. R. A. GENTRY, private communication, 1971.
4. V. A. AMBARTSUMIAN, "Theoretical Astrophysics" (translated by J. B. Sykes), Pergamon Press, London, England, 1958.
5. C. W. ALLEN, "Astrophysical Quantities," The Athlone Press, London, England, 1964.
6. C. J. EVERETT AND E. D. CASHWELL, Los Alamos Scientific Laboratory report LA-5061-MS.
7. H. G. HORAK, private communication, 1971.
8. M. T. SANDFORD II, "Indiana University Astronomy Algorithms," unpublished, 1972.
9. A. SOLEM, "Programmer's Information Manual, **5**," Los Alamos Scientific Laboratory, 1971.
10. J. A. FLECK, private communication, 1972.
11. A. S. EDDINGTON, "The Internal Constitution of the Stars," Dover Publications, New York NY, reprinted 1959.
12. G. A. SPANIER AND E. M. GELBARD, "Monte Carlo Principles and Neutron Transport Problems," Addison Wesley, Reading, MA, 1969.
13. A. L. MERTS AND N. H. MAGEE, JR., private communication, 1972.
14. R. A. HARRIS AND L. SULLO, "ABSCO — A Computer Program which Calculates and Displays Locally Integrated Planck Means," Air Force Weapons Laboratory report SYT TN 70-17, 1971.
15. YA. B. ZEL'DOVICH AND YU. P. RAIZER, "Physics of Shock Waves and High Temperature Hydrodynamic Phenomena," Academic Press, New York, 1967.